

DARK MATTER MASS LOSS IN GALAXY FLYBYS: DEPENDENCE ON IMPACT PARAMETER

A. Mitrašinović^{1,2}

¹*Astronomical Observatory, Volgina 7, 11060 Belgrade 38, Serbia*

²*Department of Astronomy, Faculty of Mathematics, University of Belgrade,
Studentski trg 16, 11000 Belgrade, Serbia*

E-mail: amitrasinovic@aob.rs

(Received: September 15, 2021; Accepted: January 26, 2022)

SUMMARY: Galaxy flybys, interactions where two independent halos inter-penetrate but detach at a later time and do not merge, occur frequently at lower redshifts. These interactions can significantly impact the evolution of individual galaxies - from the mass loss and shape transformation to the emergence of tidal features and formation of morphological disc structures. The main focus of this paper is on the dark matter mass loss of the secondary, intruder galaxy, with the goal of determining a functional relationship between the impact parameter and dark matter mass loss. Series of N-body simulations of typical galaxy flybys (10:1 mass ratio) with differing impact parameters show that the dark matter halo leftover mass of the intruder galaxy follows a logarithmic growth law with impact parameter, regardless of the way the total halo mass is estimated. The lost mass then, clearly, follows the exponential decay law. The stellar component stretches faster as the impact parameter decreases, following the exponential decay law with impact parameter. Functional dependence on impact parameter in all cases seems universal, but the fitting parameters are likely sensitive to the interaction parameters and initial conditions (e.g. the mass ratio of interacting galaxies, initial relative velocity of the intruder galaxy, interaction duration). While typical flybys, investigated here, could not be the sole culprit behind the formation of ultra-diffuse or dark matter deficient galaxies, they can still contribute significantly. Rare, atypical and stronger flybys are worth further exploring.

Key words. Galaxies: evolution – Galaxies: interactions – Methods: numerical

1. INTRODUCTION

Galaxy flybys are interactions where two independent halos inter-penetrate but detach at a later time, thus not resulting in a merger. This definition was introduced by [Sinha and Holley-Bockelmann \(2012\)](#), making a clear distinction between galaxy flybys and close galaxy passages where two halos remain separate at all times. The authors based their analysis on cosmological N-body simulations and found that

the number of flybys can even surpass the number of mergers on lower redshifts ($z \lesssim 2$). The follow-up study ([Sinha and Holley-Bockelmann 2015](#)) further explored interaction parameters: in a majority of flybys, the secondary halo penetrates deeper than $\sim R_{\text{half}}$ with the initial relative velocity $\sim 1.6 \times V_{\text{vir}}$ of the primary halo. The typical mass ratio of interacting galaxies was found to be ~ 0.1 at high redshifts, or even lower, at the lower redshift end.

The frequency and strength of galaxy flybys suggest that these interactions have the potential to significantly impact the evolution of individual galaxies, with the strongest contribution at the present epoch ([An et al. 2019](#)). The focus of previous studies was predominantly on the primary (more massive) galaxy.

© 2022 The Author(s). Published by Astronomical Observatory of Belgrade and Faculty of Mathematics, University of Belgrade. This open access article is distributed under CC BY-NC-ND 4.0 International licence.

It was established that flybys can trigger or speed up bar formation (Lang et al. 2014, Lokas 2018), create warps at the edges of the galactic disk, both gaseous and stellar (Kim et al. 2014) or, in general, reproduce diverse morphology of observed galaxies with differing interaction parameters (Pettitt and Wadley 2018).

However, effects on the secondary, intruder galaxy are equally (if not more) important, given the fact that the majority of morphological disturbances seen in dwarf galaxies ($M_* < 10^9 M_\odot$) are primarily the result of interactions like these that do not end in a merger (Martin et al. 2021). This is particularly noticeable in galaxy clusters. Tormen et al. (1998) reported that very close, penetrating encounters between satellites within the cluster are frequent, with almost 60% of satellites experiencing at least one such event before losing 80% of their initial mass. They noted that mass loss, which follows these interactions, is comparable to the one caused by global tides. Thus, interactions within galaxy clusters can contribute to the dynamical evolution of individual galaxies as equally as the global, collective effects of the cluster itself. Gnedin (2003) confirmed this by finding that peaks of the tidal force do not always correspond to the closest approach to the cluster centre but, instead, to the local density structures (e.g. massive galaxies or the unvirialized remnants of infalling groups of galaxies).

Dark matter halos of tidally affected galaxies, due to their extended nature, usually suffer significant mass loss - their outermost parts, being loosely gravitationally bound, get stripped first. With prolonged tidal effects or stronger tidal forces, the inner parts become affected and prone to the tidal stripping. Since tidal forces remove mass from outside in, the process is known as outside-in tidal stripping (e.g. Diemand et al. 2007, Choi et al. 2009). At the same time, the stellar counterpart is barely affected (Smith et al. 2015, 2016). Stripping and mass loss of the stellar component typically only starts happening after a significant portion of dark matter ($\sim 80\%$) is already lost (Smith et al. 2016, Lokas 2020). Tidal stripping, in general due to its outside-in nature, is known to be one of the formation mechanisms of ultra-compact dwarfs (Bekki et al. 2001, 2003, Pfeffer and Baumgardt 2013, Pfeffer et al. 2014, Martinović and Micic 2017, Ferré-Mateu et al. 2018, Kim et al. 2020), and there is growing evidence for tidal origin of ultra-diffuse galaxies (Carleton et al. 2019, Iodice et al. 2021, Jones et al. 2021, Wright et al. 2021). This is all reflected in a stellar-to-halo mass relation (Niemiec et al. 2017, 2019, Engler et al. 2021) - galaxies in high-density environments, such as clusters, tend to have smaller (than expected) halo masses for a given stellar mass. Exotic class of dark matter deficient galaxies can be considered as an extreme example of these mechanisms (Ogiya 2018, Montes et al. 2020, Shin et al. 2020, Jackson et al. 2021, Macciò et al. 2021, Trujillo-Gomez et al. 2022).

The aim of this paper is to explore the role of impact parameter (which will also be referred to as the pericentre distance) in galaxy flybys, with emphasis on the dark matter mass loss of the secondary, intruder galaxy. The main goal is to answer the question - is there a functional relationship between the impact parameter and dark matter mass loss of the secondary galaxy and, if so, what does it look like? This will be done by utilizing a series of N-body simulations of galaxy flybys with differing impact parameter (described in Section 2). The total dark matter mass of the intruder galaxy after the encounter will be estimated using three different criteria described in Subsection 2.2. As mass loss of the stellar component is not expected, it will be verified if that is the case and, if so, the changes to its half-mass radius will be explored. Results will be outlined and briefly discussed in Section 3. Finally, Section 4, besides drawing conclusions, will tackle potential issues of this work and will discuss the open questions.

2. MODELS, SIMULATIONS AND METHODS

Two galaxy models were constructed using the `GalactICs` software package (Kuijken and Dubinski 1995, Widrow and Dubinski 2005, Widrow et al. 2008). The primary galaxy model (which will be referred to as galaxy) consists of the NFW (Navarro et al. 1996) dark matter halo, exponential stellar disc and Hernquist (1990) stellar bulge. The dark matter halo, consisting of $N_H = 6 \cdot 10^5$ particles, has the total mass $M_H = 9.057 \cdot 10^{11} M_\odot$, scale length $a_H = 13.16$ kpc, and concentration parameter $c = 15$. The exponential stellar disc, consisting of $N_D = 3 \cdot 10^5$ particles, has the total mass $M_D = 7.604 \cdot 10^{10} M_\odot$, scale length $R_D = 5.98$ kpc, scale height $z_D = 0.688$ kpc, and central velocity dispersion $\sigma_{R_0} = 98.9$ km s $^{-1}$. The stellar bulge, consisting of $N_B = 1 \cdot 10^5$ particles, has the total mass $M_B = 2.502 \cdot 10^{10} M_\odot$, and scale radius $R_B = 2.182$ kpc.

The secondary galaxy model (which will be referred to as intruder) consists only of the NFW dark matter halo, and stellar bulge, to mimic (dwarf) a spherical galaxy for the sake of simplicity. The intruder model was scaled to be 10 times smaller than the galaxy model, in both the number of particles and total mass. This results in a dark matter halo with $N_H = 6 \cdot 10^4$ particles, $M_H = 9.044 \cdot 10^{10} M_\odot$ total mass, $a_H = 4.578$ kpc scale length, and $c = 20$ concentration parameter. The stellar component has, thus, $N_S = 4 \cdot 10^4$ particles, and $M_S = 1.022 \cdot 10^{10} M_\odot$ the total mass with scale radius $R_B = 3.145$ kpc. The relevant parameters for both galaxies are listed in Table 1.

The flyby simulations, originally designed to follow the evolution of the primary galaxy disc long after the encounter in Mitrašinović and Mičić (in prep), were performed using the publicly available code `GADGET2` (Springel 2005) compiled with the op-

Table 1: List of relevant parameters for two galaxy models where the first block is related to the dark matter halo, the second one to stellar bulge and the third to stellar disc.

	Primary galaxy	Secondary galaxy
N_{H}	$6 \cdot 10^5$	$6 \cdot 10^4$
M_{H}	$9.057 \cdot 10^{11} M_{\odot}$	$9.044 \cdot 10^{10} M_{\odot}$
a_{H}	13.16 kpc	4.578 kpc
c	15	20
N_{B}	$1 \cdot 10^5$	$4 \cdot 10^4$
M_{B}	$2.502 \cdot 10^{10} M_{\odot}$	$1.022 \cdot 10^{10} M_{\odot}$
R_{B}	2.182 kpc	3.145 kpc
N_{D}	$3 \cdot 10^5$	
M_{D}	$7.604 \cdot 10^{10} M_{\odot}$	
R_{D}	5.98 kpc	
z_{D}	0.688 kpc	
σ_{R_0}	98.9 km s $^{-1}$	

tion to calculate and output the particle potential energy. The system was evolved for 5 Gyr with outputs being saved every 0.01 Gyr. The galaxy and intruder were initially set as a contact system, ie. the distance from their centers is roughly equal to the sum of their virial radii $d_0 = R_{\text{vir},1} + R_{\text{vir},2} \approx 290$ kpc, with the galaxy being static in the centre of simulation box. The intruder was set on a prograde parabolic orbit, co-planar with the galaxy disc, with the initial relative velocity $v_0 = 500$ km s $^{-1}$. Different pericentre distances (impact parameters - these terms will be used interchangeably) b were achieved in different simulations by slightly varying initial position and velocity angles. In turn, pericentre velocities are also different, while the pericentre occurs at the same time (0.56 Gyr) and duration of interaction remains the same (1.08 Gyr) in all simulations. The interaction is here defined as the time during which the dark matter halos overlap ($d \leq R_{\text{vir},1} + R_{\text{vir},2}$).

Simulation relevant parameters are listed in Table 2. Simulations were named after a rough estimate of impact parameters - evidently, they differ from actual impact parameters (column b). Based on the results of [Sinha and Holley-Bockelmann \(2015\)](#), these simulations cover deep flybys with impact parameter ranging from $0.114 \cdot R_{\text{vir},1}$ to slightly over galaxy's half-mass radius (~ 49 kpc). The mass ratio $q = 0.1$ was found to be the most common one when the redshift z is disregarded. However, the adopted initial relative velocity is higher than the most common one. [Kim et al. \(2014\)](#) used a higher initial relative velocity, $v_0 = 600$ km/s, based on the report of [Gnedin \(2003\)](#) - in the Virgo-type cluster simulation, relative velocities of interacting galaxies show a skewed distribution, peaking at ~ 350 km/s, with median ~ 800 km/s, and mean value ~ 1000 km/s. Thus, the value of $v_0 = 500$ km/s can still be considered as representative and realistic. Additionally, attractive perk of this value is that it is high enough to significantly

Table 2: List of flyby simulations where b is the pericentre distance, $R_{\text{vir},1}$ virial radius of the main galaxy, and v_b pericentre velocity.

Name	b [kpc]	$b/R_{\text{vir},1}$	v_b [km s $^{-1}$]
B30	22.50	0.114	660.14
B35	26.53	0.135	650.86
B40	30.69	0.156	641.80
B45	35.07	0.178	632.86
B50	39.62	0.201	624.25
B50	39.62	0.201	624.25
B55	44.27	0.224	616.16
B60	48.99	0.248	608.09
B65	53.72	0.272	601.28

simplify the dark matter bound mass estimate (defined in 2.2) making it possible to utilize GADGET2's calculation of potential energy.

2.1. Assessment of intruder's center

Tidally stripped dark matter particles make the determination of the intruder's centre fairly challenging. As more dark matter particles get rejected from the intruder and shift further away from it, a simple centre of mass (which comes down to calculating the plain arithmetic mean of each coordinate for equal mass particles) also shifts away from the actual centre of the intruder. To determine the location of the actual centre, a method based on particle's potential energy is employed. Since GADGET2 calculates the total potential energy, including contributions from the main galaxy, the densest 1 kpc 3 cube with intruder particles (regardless of their type, dark matter or stellar) is first filtered. Then, the filtered particle with the lowest potential energy is chosen to represent the intruder's centre. The intruder's velocity is derived using the filtered particles only.

Fig. 1 illustrates differences between these two estimates and contributions to possible errors for each component (by calculating differences between these estimates separately for dark matter and baryon particles). Despite getting considerably lower as the impact parameter increases, these differences are still significant for the dark matter halo, reaching almost 10 kpc at a later stage. Consequently, both the estimate of the dark matter halo mass and the shape of its density profile would be wrong if the classical centre of mass is used. As expected, the baryon (stellar) component appears to be unaffected and most likely retains all of its initial mass. Differences between the two centre estimates remain below 0.6 kpc at all times in all simulations. Ideally, the centre of mass for both components should be at roughly the same position pointing to the centre of the intruder galaxy as a whole. The method used here is a way to fix issues caused by the stripped particles of the dark

matter halo. Alternatively, one can centre the whole intruder galaxy on the stellar centre of mass prior to any dark matter mass estimates as the stellar component does not have significant differences between the two centre estimates.

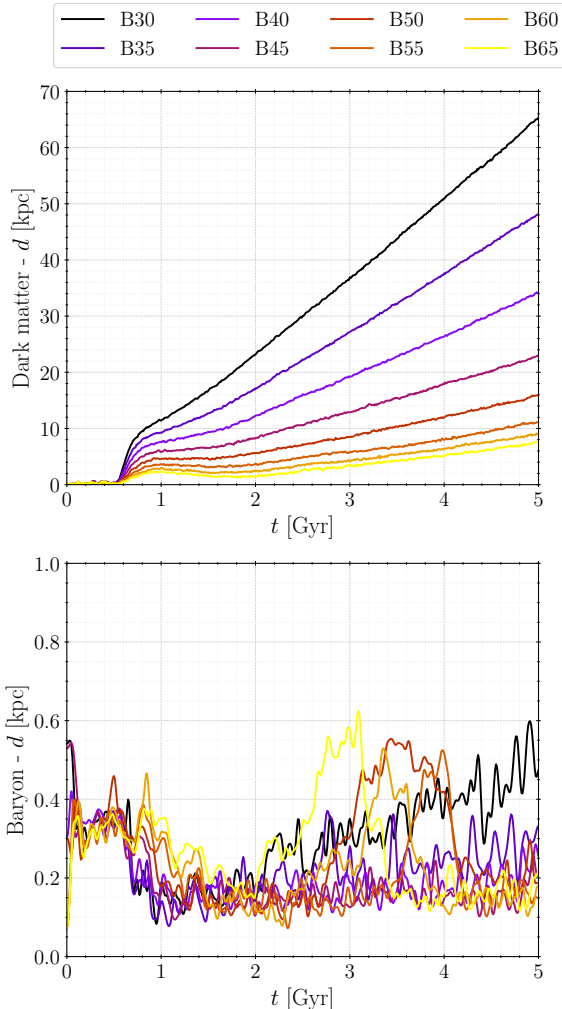


Fig. 1: Distance between two measures of intruder’s center: the simple center of mass and the lowest potential energy, for dark matter (upper panel) and baryon particles (lower panel).

2.2. Mass estimates and relevant parameters

After localizing the intruder’s centre, three different dark matter mass estimates were calculated:

- **Bound mass** measure roughly estimates the gravitationally bound mass of dark matter halo. Particle velocities are centred on the previously calculated intruder’s velocity. Then, particles with negative total energies (potential and kinetic sum) are filtered. Despite **GADGET2** calculating the total potential energy, due to a suf-

ficiently high intruder’s velocity, particles possibly captured by the primary galaxy would end up with positive total energies. However, a major pitfall of this mass measure is the inclusion of barely gravitationally bound particles forming tidal features.

- **Virial mass** filters dark matter particles inside intruder’s virial radius. Virial radius is determined by fitting the NFW profile to the intruder’s (dark matter component) density profile.
- **Core mass** measure is based on mass estimate of Klimentowski et al. (2009), Kazantzidis et al. (2011). First, the circular velocity profile is calculated as $V_{\text{circ}}(r) = \sqrt{GM(<r)/r}$, where $M(<r)$ is the cumulative mass of dark matter halo and r is the sphere radius. Radius r_{max} , where this profile reaches maximum V_{max} , is chosen as cutoff, and $M(<r_{\text{max}})$ represents the dark matter halo core mass.

By definition, at later stages of simulations, virial and core mass measures should remain fairly constant. The core mass, accounting for the majority of dark matter particles, should be seen as a lower limit for the total dark matter mass whereas the bound mass should represent an upper limit. The bound mass should continue to decline over time as tidal features slowly dissolve and the majority of particles become detached from the intruder. Some particles might get recaptured by the intruder, which would result in a slight increase in virial mass. Due to this, as the main measure of intruder’s dark matter mass, the virial mass averaged over the last 3 Gyr will be used.

The baryon (stellar) component of the intruder is not expected to lose a significant amount of mass. Moreover, based on the previous centre of mass estimates for the stellar component, it is likely that all of its particles remain within the virial radius. However, this does not imply that the stellar component does not undergo any changes. Evolution of the half-mass radius $R_{\text{B},0.5}$ will be followed. Note that, with the total stellar mass remaining constant, changes in the half-mass radius imply changes in the average spherical density of the stellar component: when the half-mass radius increases, density decreases and vice versa.

3. RESULTS

The evolution of dark matter halo mass estimates defined in 2.2 is shown in Fig. 2. These estimates are expressed in a relative form as:

$$f_M = \frac{M(t)}{M(t=0)}, \quad (1)$$

where $M(t)$ is the appropriate estimate (bound, virial or core) during simulation(s), $M(t=0)$ is its value at

the start of simulation(s), and f_M , thus, represents the leftover fraction of the initial dark matter mass. Supplementary to Fig. 2, Fig. 3 shows the evolution of the dark matter mass change rate expressed as a percentage of its initial mass per Gyr. It has to be noted that the initial values of both the bound and virial estimates, in all simulations, are equivalent to $M = 9.044 \cdot 10^{10} M_\odot$ (the initial dark matter halo total mass), while the dark matter core mass is $M = 3.684 \cdot 10^{10} M_\odot$.

As expected, a significant mass change rate is observed after the pericentre is reached for all mass estimates. During the encounter the intruder stretches, becoming heavily distorted for a brief period, which is best visible in core mass plots. The core distortion is followed by abrupt mass loss, after which the dark matter core stabilizes and remains fairly constant with negligible variations until the end of every simulation. The whole process takes place even before the encounter is over. The final leftover fraction of the dark matter core mass estimate is higher than the leftover fraction of virial mass estimate in most simulations (evident from Fig. 4 as well). This implies that despite of strong gravitational influence of the main galaxy, the core part of intruder's dark matter halo remains semi-preserved. It is also the key in understanding why the baryon component can retain almost all of its initial mass - gravitational potential of the preserved dark matter halo's core protects the baryon component against significant mass loss.

The virial mass takes longer to stabilize - while the dark matter mass loss starts around the time the pericentre is reached, mass loss rate (Fig. 3) peaks right after the encounter, at $t \geq 1.08$ Gyr. The peak itself shows dependence on the pericentre distance, ranging from $< 50\%$ of the initial dark matter mass per Gyr, in simulation with the lowest pericentre distance (B30), to $\simeq 16\%$ of the initial dark matter mass per Gyr, in simulation with the highest pericentre distance (B65). Following the peak, the mass loss rate sharply declines from $\simeq 10\%$ of the initial dark matter mass per Gyr at $t = 2$ Gyr to no mass loss at $t = 3$ Gyr in all simulations, irrespective of the pericentre distance. After $t = 3$ Gyr, there is an almost constant mass gain of $\leq 1\%$ of the initial dark matter mass per Gyr in all simulations. Thus, the most significant virial mass loss is observed for 1 Gyr following the end of the encounter. Bearing that in mind, for fitting purposes (i.e. exploring the functional relationship between the leftover virial mass and impact parameter relative to the virial radius of the primary) the virial mass fraction averaged over the last 3 Gyr will be used.

The bound dark matter mass expectedly declines until the end of each simulation. Its mass loss is much slower than the one of the virial mass, even during peak, which happens after the pericentre is reached and before the encounter is over. During the last 1 Gyr, the mass loss rate is almost constant in all simulations, varying between 1–2% of the initial dark

matter mass per Gyr. Given that the final fraction of the bound dark matter mass is still higher than the virial mass fraction at the end, and that the mass loss rate is non-zero at $t = 5$ Gyr, the bound dark matter mass will likely continue to decline past the simulation cutoff at 5 Gyr until it converges with the virial mass.

Note that the bound dark matter mass discussed here should be considered as an upper limit for the truly bound mass. Other than the inclusion of particles forming tidal features outside the virial radius, our method possibly includes dark matter particles that might not be gravitationally bound to the intruder's core. A precise determination of the bound mass would, ideally, require the use of the "snowballing" method (Smith et al. 2015). However, this method is robust and was not feasible, due to our limited computing resources.

3.1. Leftover dark matter mass - dependence on impact parameter

The leftover dark matter mass fraction, for each type of mass estimate, as a function of impact parameter (pericentre distance) relative to the virial radius of the primary, is shown in Fig. 4, with different types of mass estimates denoted by different colours. Filled circles represent simulation data, and lines represent logarithmic growth fit of the form:

$$y = A \cdot \ln x + B, \quad (2)$$

where y corresponds to the leftover dark matter mass fraction, x corresponds to the impact parameter (pericentre distance) relative to the virial radius of the primary, and A and B are fitting parameters. As evident, the virial and core leftover dark matter mass's dependence on impact parameter is perfectly described by a logarithmic growth law. The bound dark matter mass fraction, albeit deviating from the fitted line, can still be described by a logarithmic growth law. Fitting parameters are different for all three types of mass: the virial mass has $A = 0.3123$ and $B = 1.2811$, core mass has $A = 0.2069$ and $B = 1.1443$, and bound mass has $A = 0.2384$ and $B = 1.2935$. These fitting parameters are likely not universal and they depend on multiple interaction parameters, e.g. the mass ratio of interacting galaxies, the initial relative velocity of intruder galaxy, and the interaction duration.

Surprisingly, the outside-in nature of the tidal stripping, which is one of the main formation mechanisms of ultra-compact dwarf galaxies (mentioned in the introductory part of this paper), is less evident in flybys with larger impact parameters (i.e. weaker ones). Examining the extreme cases, simulation B30 with the lowest and simulation B65 with the highest impact parameter yields interesting insights. In B30, the leftover dark matter core mass fraction is by $\sim 9\%$ higher than the leftover virial mass fraction while they are almost equal in B65. Generally, the

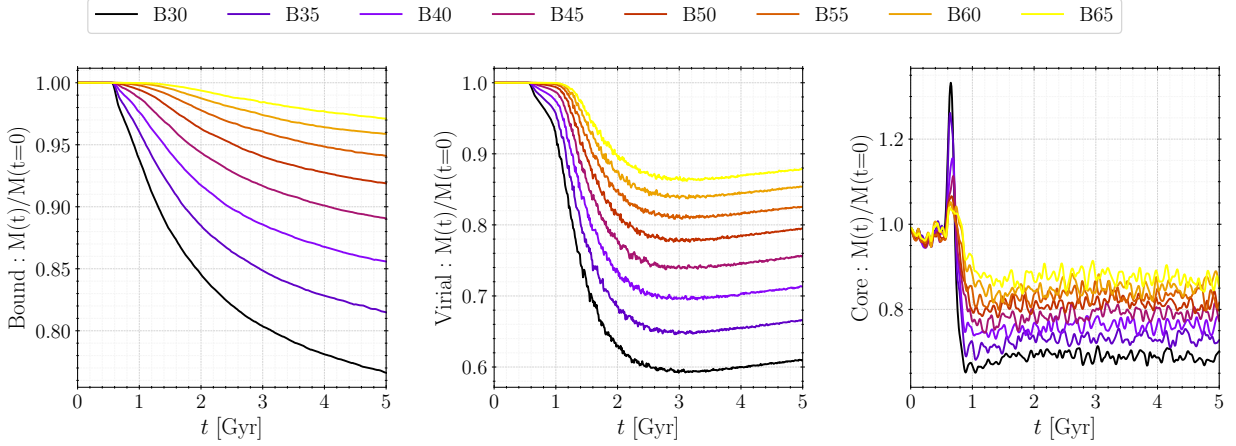


Fig. 2: Evolution of dark matter halo mass estimates defined in 2.2 (from left to right): bound (first panel), virial (second panel), core mass (third panel). Different colors are assigned to different simulations. Estimates are expressed in relative form, compared to initial mass, and thus represent fractions of leftover mass.

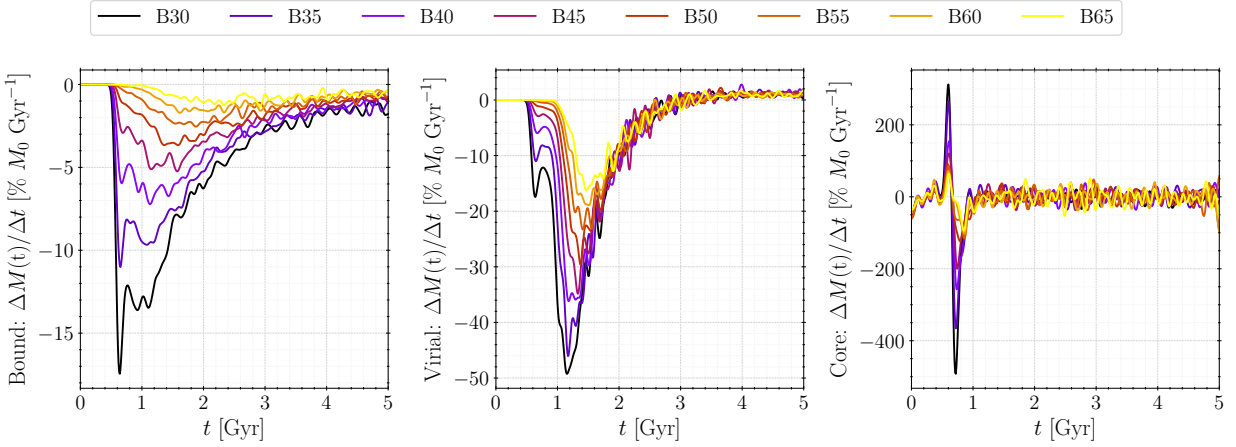


Fig. 3: Mass change rate $\Delta M/\Delta t$ for different mass estimates and simulations with the same annotations as in Fig. 2. Mass change rate is expressed as percentage of initial mass per Gyr (contrary to Fig. 2 which shows fractions).

decreasing difference between these two dark matter mass estimates with increasing impact parameter indicates that the outer parts of the dark matter halo are more affected in closer (i.e. stronger) flybys and thus lose more mass than the inner (core) parts. As the impact parameter increases, the dark matter mass loss becomes almost uniform with radius. This might lead to an assumption that density profiles, and thus shapes and slopes of the NFW profiles, are heavily affected. In reality, this is not entirely the case (Fig. 5) - while differences become visible at larger radii ($R \geq 18$ kpc), the density profiles are not significantly altered in inner parts where the majority of leftover particles reside. Normalized density profiles (relative to their fitted analytical NFW profile) are shown in the lower panel in Fig. 5. High deviations at the centre are understandable as the analytical form has unrealistically high densities in low radii ($R \rightarrow 0$). Well outside the dark matter

half-mass radius ($R \geq 18$ kpc)¹, deviations of density profiles from the analytical NFW increase drastically. The effect is more prominent in closer flybys where higher fractions of dark matter mass are stripped. This confirms that, due to the outside-in nature of the tidal stripping, the outer parts of dark matter halo density profiles are steeper than the analytical NFW (e.g. Okamoto and Habe 1999, Genina et al. 2022). Thus, the NFW does not describe the dark matter halo density profiles well overall while the approximation is still consistent in the inner parts.

Dependence of the leftover dark matter mass (of the intruder galaxy in flybys) on impact parameter is, undisputedly, perfectly described with a logarithmic

¹Half-mass radius, which encloses half of the leftover dark matter mass, varies between ~ 5.5 kpc (B30) and ~ 7.5 kpc (B65). These can be approximated for each simulation using the data listed in Table 3 - namely the leftover mass M_{DM} , virial radius $R_{\text{vir},2}$ and concentration parameter c .

growth law. Naturally, the lost mass would then follow the exponential decay law. As such, the decreasing impact parameter is followed by a considerable and ever so faster dark matter mass loss. This will be discussed in detail in Section 4 keeping in mind the constraints of this work.

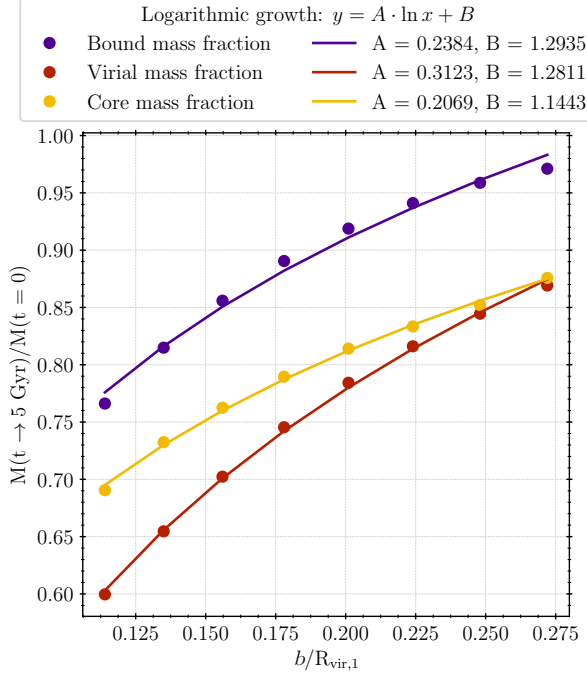


Fig. 4: Leftover mass (fraction of the initial mass) versus the impact parameter (the pericentre distance) relative to the virial radius of the primary: bound (purple), virial (red), and core mass (yellow). Filled circles represent simulation data, while lines show the logarithmic growth fit: $y = A \cdot \ln x + B$. Fitting parameters A and B are included in the legend.

3.2. Changes to stellar component and dark-to-stellar mass ratio

Contrary to the dark matter halo, the stellar component does not suffer any mass loss. The total stellar mass was estimated by applying the method for the bound dark matter mass estimate to stellar particles. Since it remains constant in all simulations, its visualisation is omitted. However, the total stellar mass remaining constant does not imply absence of changes in the stellar component. The final half-mass radius of the stellar component, $R_{0.5}$, as a function of impact parameter (relative to the virial radius of the primary), is shown in the lower panel of Fig. 6. The exponential decay law $R_{0.5} = A \cdot \exp(-B \cdot b/R_{\text{vir},1}) + C$ describes its behaviour the best with fitting parameters: $A = 2.2$, $B = 18.23$, and $C = 4.24$. While it stretches faster as the impact parameter decreases, the value of $R_{0.5} = 4.5097$ kpc in the strongest flyby

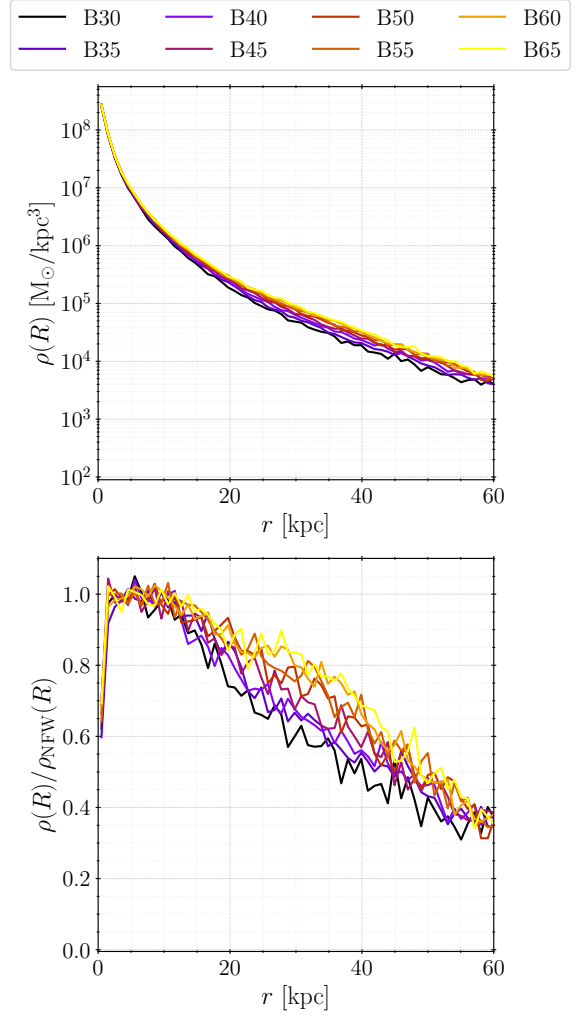


Fig. 5: *Upper panel:* Final ($t = 5$ Gyr) density profiles of the dark matter component. Different colors are assigned to different simulations. *Lower panel:* Normalized density profiles (relative to the analytical NFW profile), with the same annotations as on the upper panel.

simulation (B30) is not considerably larger than the initial one of $R_{0.5} = 4.153$ kpc. Typical flybys, hence, can contribute to the formation of ultra-diffuse galaxies but cannot be its sole formation mechanism.

Unsurprisingly, given that the stellar component does not suffer mass loss, the dark-to-stellar mass ratio M_D/M_S shown in the upper panel of Fig. 6 follows a logarithmic growth law (similar to that of the leftover virial mass), with fitting parameters $A = 2.75$ and $B = 11.32$. From the initial value of $M_D/M_S = 8.86$, this ratio drops to $M_D/M_S = 5.317$ in the most extreme case (simulation B30). Despite losing almost half of its initial dark matter mass, the intruder galaxy remains dark matter dominated, albeit less so. Variations in this ratio caused by galaxy flybys, however, can contribute to the scatter in the SHMR (stellar-to-halo mass relation) at the lower

mass end, $M_{\text{halo}} \leq 10^{11} M_{\odot}$. Scatter in the SHMR in this dwarf regime has received very little attention so far. Its importance is becoming more clear as the extreme cases could successfully explain the formation of dark matter deficient galaxies (Trujillo-Gomez et al. 2022).

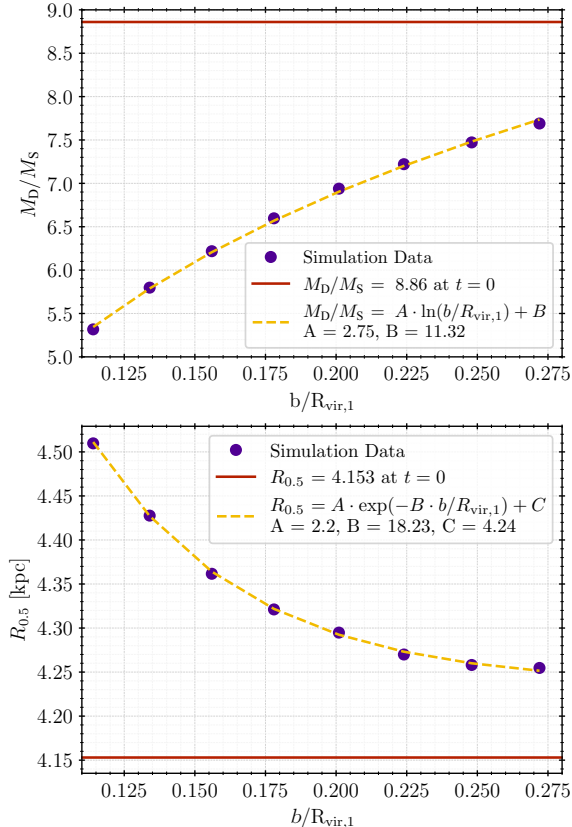


Fig. 6: In both panels, filled circles represent simulation data, solid line the initial value (at $t = 0$), and dashed line the best fit curve, with fitting functions and parameters included in the legend; all as a function of impact parameter relative to virial radius of the primary. *Upper panel:* Dark-to-stellar mass ratio, where M_D is the final (at $t = 5$ Gyr) virial mass, and M_S final mass of the stellar component. *Lower panel:* The final half-mass radius of the stellar component, $R_{0.5}$.

4. DISCUSSION AND CONCLUSION

Series of N-body simulations of typical (10:1 mass ratio) deep galaxy flybys were performed for differing impact parameters ranging from 0.114 to 0.272 of the virial radius of the primary galaxy. The focus of the analysis was on the dark matter mass loss of the secondary, intruder, galaxy, using three different methods of estimating the total dark matter mass of the intruder. Dependence on the impact parameter for all of them is a logarithmic growth in case of the leftover dark matter mass, and exponential de-

decay for the lost dark matter mass. This functional dependence seems universal, while fitting parameters may vary with different initial conditions and interaction parameters (such as the mass ratio of interacting galaxies, the initial relative velocity of the intruder galaxy and thus the interaction duration). Most relevant visualised results in this paper are listed in Table 3 as a summary.

The bound dark matter mass calculated here should be taken as an absolute upper limit of the truly bound dark matter leftover mass, given the rough nature of this estimate. Furthermore, such an estimate has very low applicability. The virial mass, conversely, is a much better indicator of intruder galaxy’s total dark matter mass as it is suitable for comparison with results and data of cosmological simulations. However, this value should be taken with a dose of scepticism due to considerable deviations of dark matter density profiles from the analytical NFW on higher radii. Still, it is not the only noteworthy dark matter mass estimate. The core dark matter mass, estimating the total mass of the inner dark matter halo, is an appropriate one for comparison with observationally derived dark matter fractions, which can typically only probe regions where baryons are present. Particularly, it is of interest that this estimate stabilizes faster than the virial one, reaching its final values even before the encounter is over. This makes it convenient to estimate, to an extent, the total virial mass and its loss which happens 1-2 Gyrs later, based on observationally derived dark matter masses. Disparities may, of course, arise due to the outside-in nature of tidal stripping, especially in closer flybys.

Typical flybys investigated here could not be the sole culprit behind the formation of ultra-diffuse or dark matter deficient galaxies, but their effects and contributions should not be disregarded. Considering their frequency at the present epoch (Sinha and Holley-Bockelmann 2012, An et al. 2019), combined with other possible close encounters and collective effects of galaxy clusters where such events are likely to take place, these scenarios become highly plausible.

Given the nature of exponential decay with impact parameter of both the lost dark matter mass and half-mass radius of the stellar component, it is fairly safe to assume that closer (or stronger in a different way, e.g. slower) flybys than the ones investigated here, could alone lead to the formation of ultra-diffuse and dark matter deficient galaxies with *just the right* impact parameters. The formation of ultra-diffuse galaxies might not require a narrow range of impact parameters. Stellar component stretches at a faster rate than the dark matter mass loss. While stretching and getting extended, it might become prone to the mass loss itself, although that usually only starts happening after a significant portion of dark matter ($\sim 80\%$) is already stripped (Smith et al. 2016, Lokas 2020). Since this was not observed even in the simulation with the closest flyby presented here, an

Table 3: List of the most relevant results where b is the pericentre distance, $R_{\text{vir},1}$ virial radius of the main galaxy, M_{DM} virial leftover mass expressed as percentage of the initial virial mass, $M_{\text{DM}}/M_{\text{B}}$ dark-to-baryon mass ratio, $R_{\text{vir},2}$ virial radius of the intruder galaxy averaged over last 3 Gyr, $\Delta R_{\text{vir},2}$ variation of intruder’s virial radius over last 3 Gyr, $R_{\text{B},0.5}$ half-mass radius of the baryon (stellar) component at the end of simulation, and c dark matter halo concentration parameter at $t = 5$ Gyr.

Name	b [kpc]	$b/R_{\text{vir},1}$	M_{DM} [%]	$M_{\text{DM}}/M_{\text{B}}$	$R_{\text{vir},2}$ [kpc]	$\Delta R_{\text{vir},2}$ [kpc]	$R_{\text{B},0.5}$ [kpc]	c
B30	22.5	0.114	59.96	5.317	87.95	0.92	4.5097	28.94
B35	26.53	0.135	65.46	5.798	89.74	1.03	4.4277	29.35
B40	30.69	0.156	70.23	6.218	92.48	1.09	4.3616	26.62
B45	35.07	0.178	74.55	6.597	93.69	1.17	4.3211	26.47
B50	39.62	0.201	78.43	6.939	94.75	1.04	4.2948	26.56
B55	44.27	0.224	81.61	7.221	95.83	1.14	4.2700	26.10
B60	48.99	0.248	84.45	7.472	96.90	1.10	4.2581	25.63
B65	53.72	0.272	86.92	7.690	97.77	1.09	4.2547	24.94

estimate of the required impact parameter for such a case would be pure speculation at this point.

The possible formation of dark matter deficient galaxies through galaxy flybys is much more sensitive. It would require flybys with extremely low impact parameters, or much slower deep flybys, in addition to the faster rate of dark matter stripping compared to stellar one. Moreover, it might require specific shapes of density profiles for both the dark matter, and baryon component. While such flybys are extremely rare, they are still detected in cosmological simulations (Sinha and Holley-Bockelmann 2015), which is in line with the exotic nature of these objects.

This is, of course, entirely speculative. The approach and methods, presented in this work, are unfit to deal with flybys with lower impact parameters. Simulations being pure N-body are rather simplified and have no way of dealing with various and complex physical processes which would occur in such interactions. Rare, atypical and stronger (in any way, with lower impact parameters, lower initial velocities or higher differences in initial masses of interacting galaxies) flybys are, however, worth further exploring. The best approach would be trying to reconcile complex hydrodynamical simulations of isolated flybys with cosmological simulations, and hopefully, observational data.

Acknowledgements – I am grateful to my mentor, Miroslav Mićić, for his immense support and patience. I would also like to thank the reviewer for the insightful comments that helped improve the quality of this work. This work was supported by the Ministry of Education, Science and Technological Development of the Republic of Serbia (MESTDRS) through the contract no. 451-03-68/2022-14/200002 made with Astronomical Observatory of Belgrade, and the contract no. 451-03-68/2022-14/200104 made with Faculty of Mathematics, University of Belgrade. The python packages MATPLOTLIB (Hunter

2007), NUMPY (Harris et al. 2020), SCIPY (Virtanen et al. 2020), PANDAS (Wes McKinney 2010), and PYNBODY (Pontzen et al. 2013) were all used in parts of this analysis.

REFERENCES

- An, S.-H., Kim, J., Moon, J.-S. and Yoon, S.-J. 2019, *ApJ*, **887**, 59
- Bekki, K., Couch, W. J., Drinkwater, M. J. and Gregg, M. D. 2001, *ApJL*, **557**, L39
- Bekki, K., Couch, W. J., Drinkwater, M. J. and Shioya, Y. 2003, *MNRAS*, **344**, 399
- Carleton, T., Errani, R., Cooper, M., et al. 2019, *MNRAS*, **485**, 382
- Choi, J.-H., Weinberg, M. D. and Katz, N. 2009, *MNRAS*, **400**, 1247
- Diemand, J., Kuhlen, M. and Madau, P. 2007, *ApJ*, **667**, 859
- Engler, C., Pillepich, A., Joshi, G. D., et al. 2021, *MNRAS*, **500**, 3957
- Ferré-Mateu, A., Forbes, D. A., Romanowsky, A. J., Janz, J. and Dixon, C. 2018, *MNRAS*, **473**, 1819
- Genina, A., Read, J. I., Fattahi, A. and Frenk, C. S. 2022, *MNRAS*, **510**, 2186
- Gnedin, O. Y. 2003, *ApJ*, **582**, 141
- Harris, C. R., Millman, K. J., van der Walt, S. J., et al. 2020, *Natur*, **585**, 357
- Hernquist, L. 1990, *ApJ*, **356**, 359
- Hunter, J. D. 2007, *Computing in Science & Engineering*, **9**, 90
- Iodice, E., La Marca, A., Hilker, M., et al. 2021, *A&A*, **652**, L11
- Jackson, R. A., Kaviraj, S., Martin, G., et al. 2021, *MNRAS*, **502**, 1785
- Jones, M. G., Bennet, P., Mutlu-Pakdil, B., et al. 2021, *ApJ*, **919**, 72
- Kazantzidis, S., Lokas, E. L., Callegari, S., Mayer, L. and Moustakas, L. A. 2011, *ApJ*, **726**, 98
- Kim, J. H., Peirani, S., Kim, S., et al. 2014, *ApJ*, **789**, 90

- Kim, S., Jeong, H., Rey, S.-C., et al. 2020, *ApJ*, **903**, 65
- Klimentowski, J., Lokas, E. L., Kazantzidis, S., Mayer, L. and Mamon, G. A. 2009, *MNRAS*, **397**, 2015
- Kuijken, K. and Dubinski, J. 1995, *MNRAS*, **277**, 1341
- Lang, M., Holley-Bockelmann, K. and Sinha, M. 2014, *ApJL*, **790**, L33
- Lokas, E. L. 2018, *ApJ*, **857**, 6
- Lokas, E. L. 2020, *A&A*, **638**, A133
- Macciò, A. V., Prats, D. H., Dixon, K. L., et al. 2021, *MNRAS*, **501**, 693
- Martin, G., Jackson, R. A., Kaviraj, S., et al. 2021, *MNRAS*, **500**, 4937
- Martinović, N. and Micic, M. 2017, *MNRAS*, **470**, 4015
- Mitrašinović, A. and Mičić, M. in prep
- Montes, M., Infante-Sainz, R., Madrigal-Aguado, A., et al. 2020, *ApJ*, **904**, 114
- Navarro, J. F., Frenk, C. S. and White, S. D. M. 1996, *ApJ*, **462**, 563
- Niemiec, A., Jullo, E., Limousin, M., et al. 2017, *MNRAS*, **471**, 1153
- Niemiec, A., Jullo, E., Giocoli, C., Limousin, M. and Jauzac, M. 2019, *MNRAS*, **487**, 653
- Ogiya, G. 2018, *MNRAS*, **480**, L106
- Okamoto, T. and Habe, A. 1999, *ApJ*, **516**, 591
- Pettitt, A. R. and Wadsley, J. W. 2018, *MNRAS*, **474**, 5645
- Pfeffer, J. and Baumgardt, H. 2013, *MNRAS*, **433**, 1997
- Pfeffer, J., Griffen, B. F., Baumgardt, H. and Hilker, M. 2014, *MNRAS*, **444**, 3670
- Pontzen, A., Roškar, R., Stinson, G. S., et al. 2013, pynbody: Astrophysics Simulation Analysis for Python, astrophysics Source Code Library, ascl:1305.002
- Shin, E.-j., Jung, M., Kwon, G., et al. 2020, *ApJ*, **899**, 25
- Sinha, M. and Holley-Bockelmann, K. 2012, *ApJ*, **751**, 17
- Sinha, M. and Holley-Bockelmann, K. 2015, [arXiv:1505.07910](https://arxiv.org/abs/1505.07910)
- Smith, R., Sánchez-Janssen, R., Beasley, M. A., et al. 2015, *MNRAS*, **454**, 2502
- Smith, R., Choi, H., Lee, J., et al. 2016, *ApJ*, **833**, 109
- Springel, V. 2005, *MNRAS*, **364**, 1105
- Tormen, G., Diaferio, A. and Syer, D. 1998, *MNRAS*, **299**, 728
- Trujillo-Gomez, S., Kruijssen, J. M. D. and Reina-Campos, M. 2022, *MNRAS*, **510**, 3356
- Virtanen, P., Gommers, R., Oliphant, T. E., et al. 2020, *Nature Methods*, **17**, 261
- Wes McKinney. 2010, in Proceedings of the 9th Python in Science Conference, ed. Stéfan van der Walt and Jarrod Millman, 56 – 61
- Widrow, L. M. and Dubinski, J. 2005, *ApJ*, **631**, 838
- Widrow, L. M., Pym, B. and Dubinski, J. 2008, *ApJ*, **679**, 1239
- Wright, A. C., Tremmel, M., Brooks, A. M., et al. 2021, *MNRAS*, **502**, 5370

ГУБИТАК МАСЕ ТАМНЕ МАТЕРИЈЕ У ПРОЛЕТИМА ГАЛАКСИЈА: ЗАВИСНОСТ ОД ПАРАМЕТРА СУДАРА

A. Mitrašinović^{1,2}

¹*Astronomical Observatory, Volgina 7, 11060 Belgrade 38, Serbia*

²*Department of Astronomy, Faculty of Mathematics, University of Belgrade,
Studentski trg 16, 11000 Belgrade, Serbia*

E-mail: amitrasinovic@aob.rs

УДК 524.7–423

Оригинални научни рад

Пролети галаксија, интеракције где два независна халоа међусобно продиру један у други, али се затим одвоје и не сударе, су честа појава на нижим црвеним помацима. Ове интеракције могу имати значајан утицај на еволуцију појединачних галаксија, почев од губитка масе и промена облика галаксија, па до појаве последица плимских ефеката и формирања различитих морфолошких структура у дисковима галаксија. Главни фокус овог рада је на губитку масе тамне материје секундарне, галаксије "уљеза", са циљем одређивања функционалне зависности губитка масе тамне материје од параметра судара. Серија симулација N тела типичних пролета галаксија (однос маса 10:1) са различитим параметрима судара, показује да преостала маса тамног халоа галаксије "уљеза" прати закон логаритамског раста са параметром судара, без обзира на начин на који је укупна

маса процењена. Изгубљена маса онда, јасно, експоненцијално опада. Звездана компонента се брже шири са смањењем параметра судара, пратећи закон експоненцијалног пада. Функционална зависност од параметра судара у свим случајевима се чини универзалном, али су њени одговарајући параметри вероватно осетљиви на параметре интеракције и почетне услове (нпр. однос маса интерагујућих галаксија, релативна почетна брзина галаксије "уљеза", трајање интеракције). Док типични пролети, проучавани овде, не могу бити једини узрочник формирања ултра-дифузних галаксија, или галаксија без велике количине тамне материје, њихови ефекти не смеју бити игнорисани јер могу у знатној мери допринети овим појавама. Стога су ретки, нетипични, и јачи пролети вредни даљег и детаљнијег истраживања.